

Active Nucleosome Displacement: A Theoretical Approach

Laleh Mollazadeh-Beidokhti,[†] Farshid Mohammad-Rafiee,[†] and Helmut Schiessel^{†*}

[†]Physics Department, Institute for Advanced Studies in Basic Sciences, Zanjan, Iran; and [†]Instituut-Lorentz, Universiteit Leiden, Leiden, The Netherlands

ABSTRACT Three-quarters of eukaryotic DNA are wrapped around protein cylinders forming so-called nucleosomes that block the access to the genetic information. Nucleosomes need therefore to be repositioned, either passively (by thermal fluctuations) or actively (by molecular motors). Here we introduce a theoretical model that allows us to study the interplay between a motor protein that moves along DNA (e.g., an RNA polymerase) and a nucleosome that it encounters on its way. We aim at describing the displacement mechanisms of the nucleosome and the motor protein on a microscopic level to understand better the intricate interplay between the active step of the motor and the nucleosome-repositioning step. Different motor types (Brownian ratchet versus power-stroke mechanism) that perform very similarly under a constant load are shown to have very different nucleosome repositioning capacities.

INTRODUCTION

Three-quarters of eukaryotic DNA are tightly associated with octamers of histone proteins that serve as cores of DNA spools. For each resulting complex, called the nucleosome, a 147-basepairs' (bp) long stretch of DNA is wrapped in 1.75 left-handed superhelical turns around the histone octamer resulting in a 6-nm-high cylinder of 5-nm radius (1). This leads to the intriguing questions of how eukaryotes can then expose their DNA to DNA binding proteins, how entire genes (typically associated with tens of nucleosomes) can be transcribed, and how DNA can be replicated.

Some answers to these questions are given by the experimental observation that nucleosomes are highly dynamic complexes that transiently expose their associated DNA to other proteins (2). The two major modes that have been identified are the transient unwrapping of parts of the DNA (3,4) and the sliding of the nucleosome along DNA (5–7). Thermal fluctuations are sufficiently large to induce these mechanisms, at the same time keeping the integrity of the nucleosome. The DNA unwrapping or breathing seems typically to stop once one DNA turn is left on the nucleosome (3). This has been interpreted to result from an effective repulsion of the two DNA turns (first-, second-round difference) that stabilize the remaining turn against further unwrapping (8) and explains the experimental observation, that for a nucleosome under an external tension, the remaining turn comes off only at rather large forces (9,10). The other mode for exposure of nucleosomal DNA, the nucleosome sliding, has to rely on defects that tunnel through the nucleosome, since rigid-body sliding of the wrapped DNA around the octamer would be too costly (2).

Two types of such defects have been discussed in the literature: loop defects and twist defects (2,11). A loop can be

formed when a partially unwrapped DNA rewraps imperfectly, leaving a DNA bulge on the nucleosome. The cheapest loop has an extra length of 10 bp that corresponds to the DNA helical pitch (12,13). Loops that successfully transverse the nucleosome induce 10-bp-long steps of the octamer along the DNA. On the other hand, twist defects carry only an extra or a missing bp (14). Twist defects on the nucleosome are localized between two neighboring DNA binding sites, i.e., between two sites where the DNA minor groove touches the octamer. Successful twist defects induce 1-bp steps of the nucleosome. Since the minor groove always remains attached to the binding sites on the octamer, in this mechanism, the DNA acts as a molecular corkscrew.

Estimates show that twist defects are much cheaper than loop defects (roughly $9 k_B T$ (14) versus $23 k_B T$ (13)) and hence nucleosome mobility should be expected to rely mainly on twist defects. This is, however, not as obvious as it seems. Very recent work shows that the vast majority of nucleosomes are localized on the DNA with the help of mechanical signals that are written down along the DNA (15). This means that the bp sequence carries two superimposed codes: the classical triplet codon one, and the nucleosome positioning one. Nucleosomes are localized on such positioning sequences by the fact that certain bp sequences have a preference to be bent around a cylinder in one direction but not in other directions. As a result, sliding of positioned nucleosomes via twist defects is energetically very costly since, to move by 10 bp, the DNA chain has to make one full corkscrew rotation forcing the chain to bend in all different (including highly costly) directions. Rough estimates indicate that repositioning of a positioned nucleosome is as fast whether it relies on twist defects or on loops since, in the latter case, the DNA can always bend in the optimal direction (14). Nucleosome repositioning experiments in the presence of certain carefully designed DNA-binding ligands (6) and their theoretical interpretation (16) indicate, however, that it is indeed the twist defects that

Submitted September 12, 2008, and accepted for publication February 17, 2009.

*Correspondence: schuessel@lorentz.leidenuniv.nl

Editor: Reinhard Lipowsky.

© 2009 by the Biophysical Society
0006-3495/09/06/4387/12 \$2.00

doi: 10.1016/j.bpj.2009.02.071

account for most of the experimentally observed nucleosomal mobility.

The fact that many nucleosomes are positioned *in vivo* (15) makes active nucleosomal displacement necessary. An obvious candidate for such an active nucleosome displacer is a transcribing RNA polymerase (RNAP): encountering a nucleosome as a road-block on its way, an RNAP might simply push the nucleosome in front of it. However, carefully designed *in vitro* experiments seem to indicate that transcribing RNAPs (from bacteriophages or from eukaryotes) can tunnel through a nucleosome in a loop (17,18). Such experiments need, however, to be interpreted with care since so far they work only successfully for short DNA constructs with one positioned nucleosome. Finite size effects might very well lead to artifacts. There is indeed the possible alternative explanation (16) that the polymerase does not tunnel through the nucleosome but pushes it forward. Because of the finite DNA length, the nucleosome is recaptured by the other DNA end before it falls off the template. The result of this process is a nucleosome that has effectively moved upstream, which looks precisely as if the polymerase has gotten around the nucleosome in a loop. This interpretation of the experiments is more consistent with the observation that in the presence of DNA-binding ligands nucleosomes are immobilized, and an RNAP stalls once it encounters such a nucleosome (6). In short, according to our interpretation all the experimental findings indicate that an RNAP can push a nucleosome in front of it.

In addition, a cell provides a large class of more professional nucleosome pushers and/or pullers: the chromatin remodelers. The precise mechanisms used by those machines are still under debate (19), but it is known that they consume ATP to actively reposition nucleosomes.

The purpose of this article is to provide a microscopic description of passive and active nucleosome repositioning. We go beyond a previous study that considered this set of problems on a mean-field and linear response level (16). To do so, we introduce models for the motor protein and the nucleosome that account for some of their microscopic degrees of freedom. The two models will then be coupled together, allowing us to study what happens if a motor protein encounters a nucleosome. More specifically, as our motor protein we shall use an RNAP that is either propelled by a ratchet or a power-stroke (PS) mechanism using the well-studied Jülicher-Bruinsma toy model (20). For the nucleosome, we assume that its mobility relies on twist defects, and accounts for each defect and its interaction with other defects explicitly. This will allow us to discuss the response of the nucleosome to an externally applied force of any strength and to, e.g., examine saturation effects at higher forces. In the coupled polymerase-nucleosome problem, we shall demonstrate that the two propulsion mechanisms perform very differently in displacing nucleosomes despite showing similar force-velocity characteristics. This illustrates the necessity of using detailed models when discussing this set of problems.

The article is organized as follows. In the following section, we present the models that we use to study RNAP translocation along DNA and nucleosome repositioning in the presence of an external force. Furthermore, we discuss how we couple the two models to investigate active nucleosome repositioning. In Results, we first discuss the force-velocity curves of a transcribing polymerase where we have tuned the parameters such that the curves look similar for both mechanisms. We study the behavior of nucleosomes under a constant force and then go to the coupled system, RNAP plus nucleosome. In particular, we ask the question whether the behavior of the combined system can be predicted from the behavior of the RNAP and the nucleosome alone. We provide our Conclusions at the end of the article.

The model

Here we set up a model for the interaction between a nucleosome and a motor protein that repositions it. The motor protein could either represent a chromatin remodeler that purposely shifts the nucleosome or a transcribing RNAP, for which a nucleosome constitutes a hindrance. In the following, we will always refer to the motor as an RNAP, keeping in mind that it also could represent other molecular motors.

RNAP model

RNAPs are enzymes responsible for the synthesis of RNA transcripts. The size and number of subunits vary between species. As an example, the crystal structure of a bacterial RNAP (21) shows an enzyme of $15 \text{ nm} \times 11.5 \text{ nm} \times 11 \text{ nm}$ with a deep, 2.7-nm-wide cleft that creates an overall claw shape. After binding of the polymerase to a promoter sequence on the DNA, it begins to transcribe the DNA. The DNA inside the RNAP is melted, forming a transcription bubble. The melting occurs at the front site F of the enzyme (see schematic, Fig. 1). At the catalytic site C, where the DNA and the nascent RNA strand are bound to the RNAP, the polymerization reaction happens and a ribonucleoside triphosphate (NTP) is added to the RNA chain under release of phosphate (PPi). At another site T (tight binding site), the RNA is strung out of the RNAP. Finally at the end of the polymerase, the two strands of the DNA are bound to each other again.

It is still a question how the chemical catalysis in the RNAP is coupled to its mechanical translocation. There are two basic schemes (20,22): the Brownian ratchet (BR) (23–26) and the PS mechanism (27–29). According to the BR scheme, thermal energy causes the RNAP to go back and forth on the DNA template, and this fluctuation is biased by the addition of the next NTP to the RNA strand (23). On the other hand, in the PS case, chemical energy released from the polymerization reaction causes the RNAP to go forward. The PS mechanism is supported by crystallographic data of the RNAP (27–29). According to this model, the

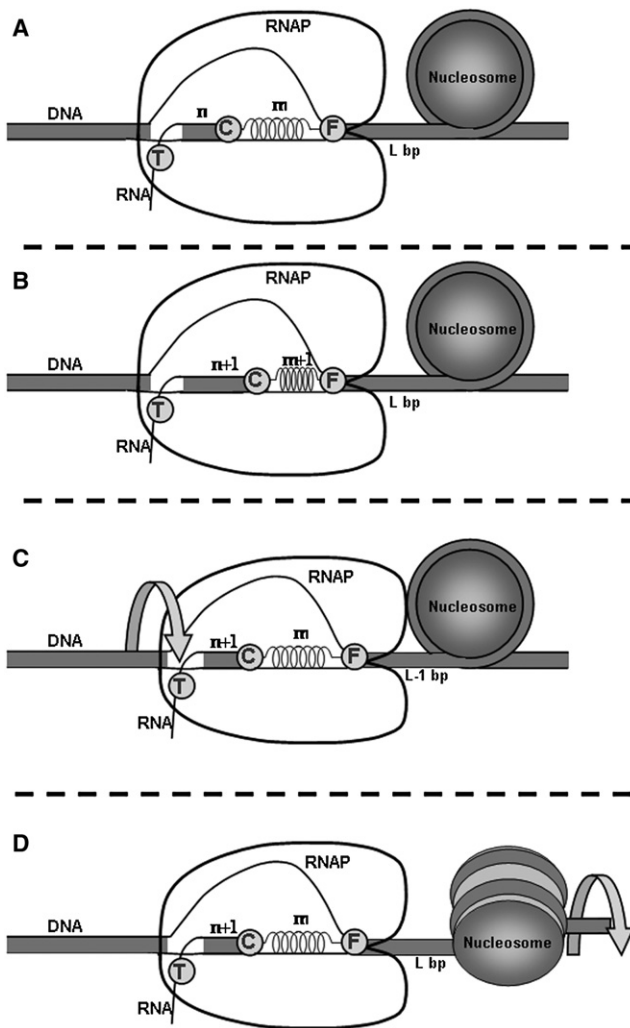


FIGURE 1 Schematic view of our model. Shown is a sequence of steps that may also happen in a different order. (A) The RNAP and the nucleosome are separated by a distance L of DNA. (B) One NTP is added to the growing RNA chain at the catalytic site C that moves 1 bp to the right. This induces an internal deformation of the RNAP (modeled by the compression of a spring). The front site, F, stays fixed. (C) The site F moves 1 bp to the right, relaxing the internal strain of the RNAP. The RNAP comes into direct physical contact with the nucleosome. The DNA stretch between the RNAP and nucleosome is shortened by 1 bp and might now be under tension. (D) This helps inject a kink into the nucleosome that eventually induces a repositioning step of the nucleosome by 1 bp. As a result, the whole system, RNAP and nucleosome, has moved 1 bp to the right, at the same time making a 36° rotation around the DNA.

RNAP has a conformational change using the energy of PPI release, thereby converting chemical energy of the polymerization reaction to the mechanical work that, in turn, translocates the polymerase along the DNA.

We represent the RNAP by the toy model of Jülicher and Bruinsma (20). In that model, one considers two crucial sites on the motor complex, the site F where the DNA enters the RNAP and the catalytic site C (at bp n) where the RNA is polymerized (Fig. 1 *a*). These two sites are assumed to be connected by a spring that models an internal flexibility of

the enzyme; the spring deformation is measured in terms of the integer variable m (in bps). Following Jülicher and Bruinsma (20), we assume an elastic energy $\varepsilon(m) = \alpha m^2$ with an elastic constant α . If the site F acts as a clamp, a polymerization step (n to $n + 1$) is accompanied by a compression of the spring (m to $m + 1$) (as some experiments suggest (30)). Hence, two correlated steps lead to the overall movement of the polymers:

Step 1. The movement of site C with F fixed, (n, m) to ($n + 1, m + 1$), with rate k_C^+ that is equivalent to the polymerization step.

Step 2. The movement of site F, (n, m) to ($n, m - 1$), with rate k_F^+ that represents the enzyme relaxation step.

The corresponding backward rates are denoted by k_C^- and k_F^- . Here we consider for simplicity no sequence sensitivity of the motor (i.e., no n -dependence of the rates). Now, suppose an external force f is exerted on the DNA (e.g., by fixing the polymerase to a substrate and applying a force to the DNA, as done in (22)). The force will be divided into two parts exerted on sites C and F: $f = f_F + f_C$. This division depends on details of the DNA-RNAP interactions. Using the condition of detailed balance, one obtains

$$\frac{k_i^+}{k_i^-} \propto e^{-af_i/k_B T}, \quad (1)$$

where a is the length of each step (1 bp for RNAP) and $i = C, F$. The difference between the two mechanisms, PS and BR, results from different ways the force affects the polymerization rate. In the PS mechanism, the polymerization at C does not involve strain coupled to the external force and the forward motion of site C will thus take place independent of the external force as

$$k_C^+(m) = k_{ps}^+(m), \quad (2)$$

$$k_C^-(m + 1) = k_{ps}^-(m + 1)e^{af_C/k_B T}. \quad (3)$$

Here, k_{ps}^\pm values are the characteristic rates of the motion of site C in the absence of external forces. The BR mechanism has to rely on thermal fluctuations that move the catalytic site by one full bp against the force before polymerization can take place. Such a step happens with a probability proportional to $\exp(-af_C/k_B T)$, and hence the BR mechanism,

$$k_C^+(m) = k_{br}^+(m)e^{-af_C/k_B T}, \quad (4)$$

$$k_C^-(m - 1) = k_{br}^-(m - 1), \quad (5)$$

where k_{br}^\pm values denote the characteristic BR rates of the motion of site C in the absence of an external force.

For both mechanisms the forward motion of C consists of a polymerization reaction together with a deformation in the RNAP. Thus, the values of the characteristic rates k_{ps}^\pm and k_{br}^\pm depend on the free energy released from the

polymerization reaction and on the change of elastic deformation of the RNAP. For the PS mechanism, this leads to

$$k_{\text{ps}}^+(m) = \eta, \quad (6)$$

$$k_{\text{ps}}^-(m+1) = \eta e^{(-\Delta\mu + \Delta\varepsilon(m))/k_{\text{B}}T}, \quad (7)$$

where η is a parameter that depends on the [NTP] and [PPi] concentrations, $\Delta\mu$ is the free energy gain per polymerization step, and $\Delta\varepsilon(m) = \varepsilon(m+1) - \varepsilon(m)$ is the elastic energy that builds up during the polymerization step. On the other hand, for the BR mechanism there is a strain-dependent potential barrier in front of site C (20):

$$k_{\text{br}}^+(m) = \eta e^{-\Delta\varepsilon(m)/k_{\text{B}}T}, \quad (8)$$

$$k_{\text{br}}^-(m+1) = \eta e^{-\Delta\mu/k_{\text{B}}T}. \quad (9)$$

The rates of the movement of site F are of the same functional form for both mechanisms (20),

$$k_{\text{F}}^+(m+1) = k^+(m+1)e^{-af_{\text{F}}/k_{\text{B}}T}, \quad (10)$$

$$k_{\text{F}}^-(m) = k^-(m), \quad (11)$$

where the constants $k^{\pm}(m)$ account for the RNAP deformation:

$$\frac{k^+(m+1)}{k^-(m)} = e^{\Delta\varepsilon(m)/k_{\text{B}}T}. \quad (12)$$

This allows for the form of $k^{\pm}(m)$ as

$$k^+(m+1) = \eta' e^{\theta\Delta\varepsilon(m)/k_{\text{B}}T}, \quad (13)$$

$$k^-(m) = \eta' e^{(\theta-1)\Delta\varepsilon(m)/k_{\text{B}}T}, \quad (14)$$

where $0 \leq \theta \leq 1$ is an adjustable parameter and η' is yet another rate constant. In this article, we set $\theta = 1$.

Nucleosome sliding

A theoretical description of nucleosome repositioning via twist defects has been put forward in Kulić and Schiessel (14). A twist defect carries either a missing bp or an extra bp and can be localized between any two neighboring binding sites of the DNA to the histone octamer. We will refer to a defect with a missing bp as a kink and with an extra bp as an antikink. Such a defect can form spontaneously at either end of the wrapped DNA portion and can then hop around the nucleosome. Defects that come out at the other end of the wrapped portion induce nucleosome reposition along the DNA. Let us denote the rate of defect injection by thermal fluctuations by k_0 and the rate of defect hopping inside the nucleosome by r_0 . Then the ratio of these two rates follows from detailed balance,

$$\frac{k_0}{r_0} = e^{-U_{\text{defect}}/k_{\text{B}}T}, \quad (15)$$

where U_{defect} is the energetic cost for a single defect (14).

Now we include into our model the effect of an external force f acting on the nucleosome. Forces can be applied to a nucleosome via at least two experimental strategies: using nanopores (31) and using a second DNA chain as a scanning probe (32). If one pulls a DNA chain through a nanopore that has a larger diameter than that of a DNA double-helix but smaller than that of a nucleosome, one can apply controlled forces on the nucleosome. In the other case, one has a setup with four optical traps and wraps one DNA chain tightly around a second, allowing us to scan along that second chain. It is not immediately obvious how such a force influences the dynamics of the nucleosome, i.e., how the rates k_0 and r_0 depend on f . It turns out that the 10-bp stretches of DNA between nucleosomal binding sites are much softer than the flexibilities of the binding site themselves; our estimates (14) indicate that a 10-bp stretch is effectively approximately five times softer, so that the outmost binding site feels 5/6 of the applied force and only 1/6 propagates into the nucleosomes. It is hence a good approximation to incorporate the effect of the external force only into the defect injection and ejection terms, but leave the internal hopping rates unaffected.

Assume now that there is a force f pulling on the left DNA arm to the left (see the nucleosome in Fig. 1 but without the RNAP present) and that the octamer is held in position. Then the formation of kinks at this left end becomes easier whereas the formation of antikinks is more costly. The ratio of the force-dependent injection and exit rates follows from detailed balance $k_{\text{esc}}(f)/k_{\text{inj}}(f) = (r_0/k_0)\exp(\mp af/k_{\text{B}}T)$ with the negative (positive) sign for kinks (antikinks) where $\mp a$ is the length stored in one defect. If we then assume that the top of the barrier for an (anti)kink escape is half-way, we find for the injection and exit rates

$$k_{\text{esc}}(f) = r_0 e^{\mp fa/2k_{\text{B}}T}, \quad (16)$$

$$k_{\text{inj}}(f) = k_0 e^{\pm fa/2k_{\text{B}}T}. \quad (17)$$

The negative (positive) sign in Eq. 16 refers to the escape and the positive (negative) sign in Eq. 17 corresponds to the injection of kinks (antikinks). Since there is no force acting on the other end of the nucleosomes, the rates are given by the same equations but with $f = 0$.

When there is no external force, injections and ejections of defects happen symmetrically on both sides and the nucleosome diffuses freely to the right and the left (as discussed in (14)). In the presence of a force, the injection rate for kinks from the left is larger than any other defect injection rate and also their exit rate to the left is the smallest. This leads to an overall flux of kinks to the right, causing the nucleosome to drift to the right.

Defect hopping inside the nucleosome

As mentioned in Kulić and Schiessel (14), nucleosomes will often encounter (in vitro and in vivo) sequence-dependent potentials of the form

$$U_{sd}(X) = \frac{A}{2} \left[1 - \cos\left(\frac{2\pi X}{10}\right) \right], \quad (18)$$

where X denotes the macroscopic position of the nucleosome on the DNA (given by the bp position of, for example, the central bp of the wrapped portion). For a random bp sequence, one has, on average, $A = 0$, but for a positioning sequence, the bp sequence is designed to induce an anisotropic DNA bendability. Since the nucleosome performs a corkscrew motion around the DNA, the nucleosome experiences approximately an oscillating bending potential with a 10-bp periodicity as in Eq. 18. For instance, the sea urchin 5 S positioning sequence, often used in experiments (see, e.g., (5)), has $a \sim A = 9 k_B T$.

Equation 18 gives the bending energy of the nucleosomal DNA as a function of the macroscopic DNA position. On the microscopic level of defects, the change of bending energy takes place in smaller steps as, for each hopping between two sides, only a 10-bp stretch of DNA has its bending direction rotated by 36° . Hence, during the hopping from a site m to its neighboring sites, $m + 1$ and $m - 1$, the defect feels the potential barriers as

$$U_m(X) = U_0 + \frac{m}{14} [\Delta U(X)], \quad (19)$$

$$\Delta U(X) = \pm [U_{sd}(X \pm 1) - U_{sd}(X)]. \quad (20)$$

Here U_0 denotes the energy of each barrier inside the nucleosome that results from the detachment of a binding site and local DNA deformation during barrier crossing (14). The \pm signs refer to different kind of defects (kinks or antikinks) moving in different directions (left or right); e.g., for a kink moving to the right, one has to use both plus signs. A schematic view of the potential barriers inside the nucleosome is shown in Fig. 2. The effect of the bending potential is to tilt the energy landscape with the slope $\Delta U(X)/14$. The rates of defect hopping to the left, $L(X)$, and to the right, $R(X)$, are then affected by the bending potential as

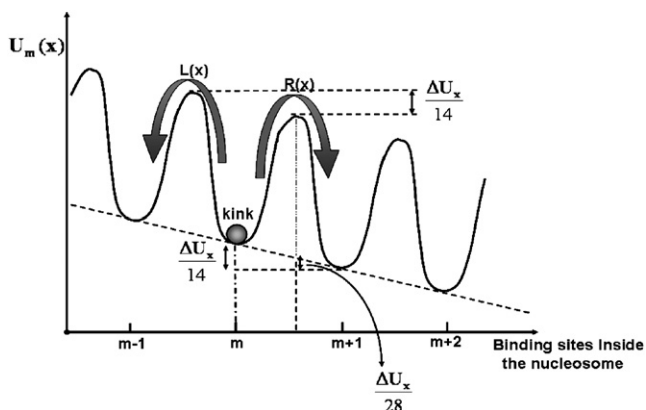


FIGURE 2 Schematic view of the potential barriers inside the nucleosome. The macroscopic position of the nucleosome on the DNA is denoted by X and the position of the potential barrier inside the nucleosome is represented by m .

$$R(X) = r_0 e^{\frac{\Delta U(X)}{28}}, \quad (21)$$

$$L(X) = r_0 e^{-\frac{\Delta U(X)}{28}}. \quad (22)$$

Note that here and everywhere else, we allow hopping of a kink (antikink) to a neighboring site only if there is not already another kink (antikink) present.

RNAP-nucleosome interaction

We assume that the nucleosome and the RNAP move independently from each other as long as their distance along the DNA is large enough. Direct physical contact sets in when the stretch of DNA between the site F of the RNAP and the DNA entry point at the nucleosome has reached a critical length L_0 whose precise value depends on the molecular shapes of the motor protein and the nucleosome. The two can move closer to each other, albeit under an energetic cost. Suppose the RNAP has reached the nucleosome and now performs another step toward the nucleosome that stays fixed at its position. Then two scenarios are, in principle, possible:

Scenario 1: Some of the DNA unwraps from the nucleosome, which again increases the length of the DNA stretch between the motor and the nucleosome (33).

Scenario 2: The nucleosome stays completely wrapped. In that case, the stretch of DNA of length L_0 extends elastically by an extra length corresponding to one bp.

In this study we will not allow for the first possibility, but mention that this effect can become important especially at higher forces (33). Instead, we will only allow for Scenario 2, i.e., an elastic deformation of the linker. This scenario will be especially dominant if at contact the mutual arrangement of the polymerase and the nucleosome leads to a locking-in of the two that hinders an unwrapping of the nucleosomal DNA.

We denote the length by which the DNA stretch between the nucleosome and the polymerase during physical contact is overstretched by x and assume that the resulting force is given by

$$f_{\text{elas}}(x) = K_{\text{eff}} x, \quad (23)$$

where K_{eff} is an effective spring constant, a combination of the twist and stretch moduli of DNA. K_{eff} depends inversely on L_0 : $K_{\text{eff}} = 1100 \text{ pN}/L_0$ (34). In the following, we take L_0 to be 10-bp-long. We have checked that the main results are not affected by the precise value of L_0 between 10 bp and 30 bp. The force in Eq. 23 opposes the motion of the RNAP and increases the rate of kink injection, biasing the nucleosome to step away from the RNAP.

RESULTS

We perform a stochastic simulation of our model using the Gillespie algorithm (35). We begin by studying the effect

of an external force on both RNAP transcription and the nucleosome sliding separately. Then we consider the full system, polymerase plus nucleosome, assuming them to be elastically coupled according to Eq. 23.

RNAP in the presence of a constant force

The RNAP model we use here has been introduced and studied in detail in Jülicher and Bruinsma (20). Here, we merely show that, for a suitable choice of parameters, the model displays force-velocity characteristics qualitatively and quantitatively similar to those observed in experiments (36,37). We especially aim at obtaining similar curves for the two mechanisms (BR and PS). This allows us later to check whether the two mechanisms still perform similarly when the RNAP encounters a nucleosome.

We use the parameters suggested in Jülicher and Bruinsma (20), namely $\Delta\mu = 10 k_B T$, $\alpha = 0.1 k_B T$, and $\eta = 6000 \text{ s}^{-1}$. The quantity η' is then used as a fitting parameter in our model. To mimic experimental curves (36,37), we set $\eta' = 0.004 \text{ s}^{-1}$ for the PS mechanism and $\eta' = 0.4 \text{ s}^{-1}$ for the BR mechanism. The higher value of η' for the BR mechanism allows for a faster enzyme strain relaxation, compensating for the fact that the polymerization reaction is slowed down by the internal stress, Eq. 8, as compared with the rate of the PS mechanism, Eq. 6.

Example trajectories of RNAP operating with the two mechanisms are depicted in Fig. 3 and are similar to experimental trajectories (36,37). The upper plot presents the trajectories in the absence of an external force, the lower plot in the presence of an opposing force of 20 pN. We show the positions of the front site F and of the catalytic site C. Note that all the sites move overall monotonously, resulting in smooth trajectories, except for the catalytic site of the PS motor that shows large and rapid oscillations. Averaging over many such trajectories, we obtain the force-velocity curves presented in Fig. 4. Note that we have tuned the parameters such that the two models feature very similar curves up to $\sim 20 \text{ pN}$ and that those curves show similar behaviors, qualitatively and quantitatively, as the experimental curves (37).

Nucleosome in the presence of a constant force

In this section we discuss the sliding of a nucleosome in the presence of an external force. We first focus on the case of random DNA, i.e., we assume that there is no position-dependent bending potential. We show that the overall outcome of the simulation can be understood in terms of a mean-field approach. In the end of the section we discuss the influence of nucleosome positioning sequence on the sliding. Throughout we use the parameter values estimated in Kulić and Schiessel (14): $U_{\text{defect}} = 10 k_B T$, $k_0 = 3 \times 10^3 \text{ s}^{-1}$, and $U_0 = 6 k_B T$.

In Fig. 5, the open triangles indicate the mean number of kinks in the nucleosome as a function of the external force. We note that, in the experimentally relevant range of a few pN, the mean number of kinks stays close to zero, reflecting

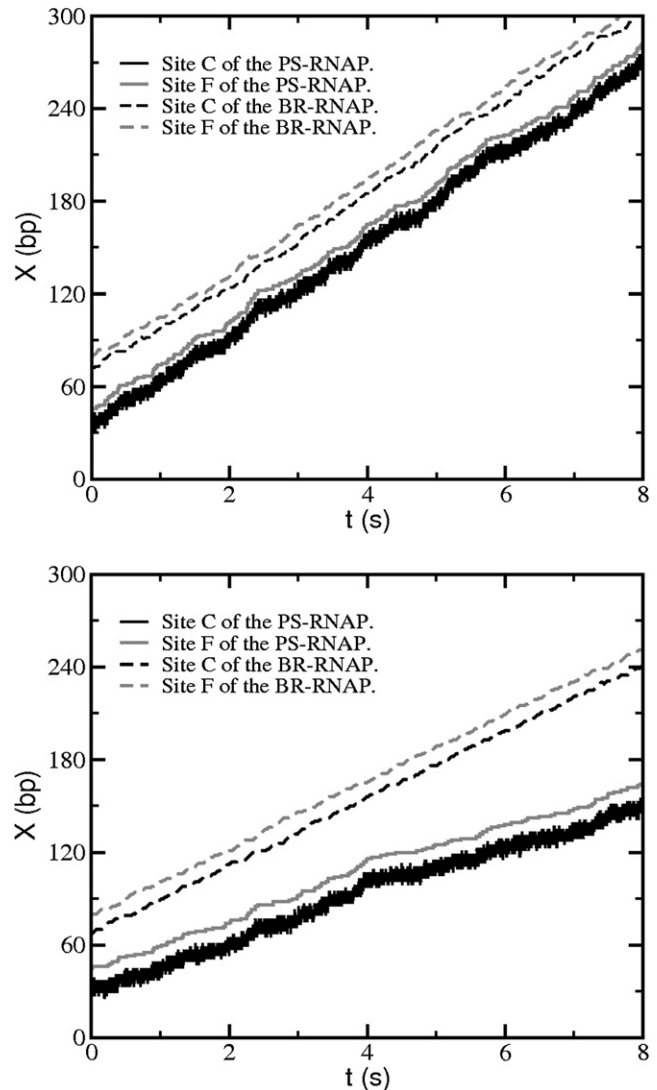


FIGURE 3 Example trajectories of RNAPs. Depicted are the positions of the catalytic site C and of the front site F as a function of time. The upper plot shows trajectories in the absence of an external force, the lower plot in the presence of an opposing force of 20 pN. Both plots compare trajectories of RNAPs that are powered by the PS and the BR mechanism, respectively.

the high cost for the formation of kink defects. The inset in Fig. 5 shows the behavior of our model for larger forces where other effects, not accounted for in our approach, would take place (e.g., DNA denaturation): beyond 100 pN, the number of kinks rises sharply, reaching a plateau of 7.5 defects at $\sim 250 \text{ pN}$.

In the following, we compare these results with a mean-field theory of this system. The master equation for the kink probability at each site obeys

$$\begin{aligned} \frac{d}{dt} \langle n_1 \rangle = & r_0 [\langle n_2 \rangle (1 - \langle n_1 \rangle) - \langle n_1 \rangle (1 - \langle n_2 \rangle)] \\ & + k_{\text{inj}}(f) (1 - \langle n_1 \rangle) - k_{\text{esc}}(f) \langle n_1 \rangle, \end{aligned} \quad (24)$$

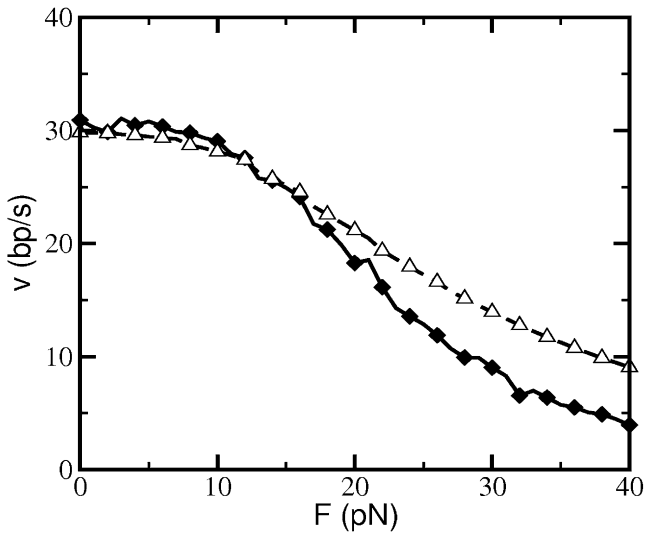


FIGURE 4 Force-velocity relation for the RNAP. The solid diamonds and the open triangles correspond to the behavior of the RNAP using PS and BR mechanisms, respectively.

$$\frac{d}{dt}\langle n_i \rangle = r_0(1 - \langle n_i \rangle)[\langle n_{i+1} \rangle + \langle n_{i-1} \rangle] - r_0\langle n_i \rangle[(1 - \langle n_{i-1} \rangle) + (1 - \langle n_{i+1} \rangle)], \quad (25)$$

$$\frac{d}{dt}\langle n_{14} \rangle = r_0[\langle n_{13} \rangle(1 - \langle n_{14} \rangle) - \langle n_{14} \rangle(1 - \langle n_{13} \rangle)] - r_0\langle n_{14} \rangle + k_0(1 - \langle n_{14} \rangle), \quad (26)$$

with $i = 2, \dots, 13$. The n_i values are two-state variables, indicating whether site i is occupied by a kink ($n_i = 1$) or is

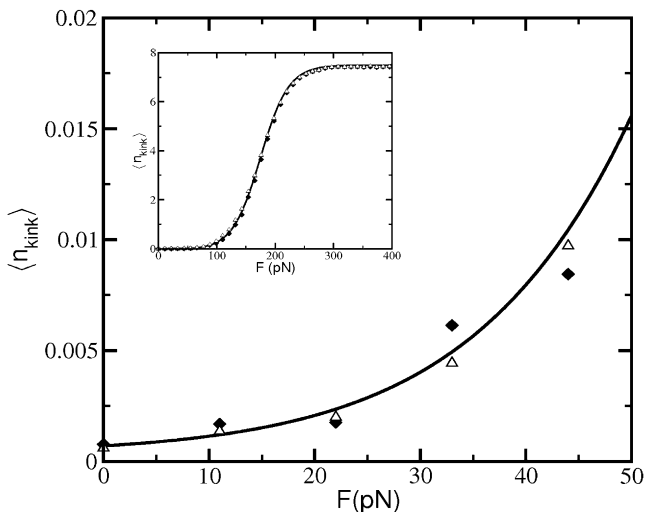


FIGURE 5 Simulation data for the mean number of defects per time step inside the nucleosome versus the external force. The open triangles correspond to random DNA and the solid diamonds to a positioning sequence with $A = 9 k_B T$. The solid curve gives the theoretical prediction, Eq. 29. The inset shows the saturation behavior of our model at large forces.

empty ($n_i = 0$). The quantity $\langle n_i \rangle$ denotes the probability to find a kink at the i^{th} site. Here we use the fact that, for random DNA, the left and right kink-hopping rates are the same, r_0 . Kink-kink repulsion is accounted for by reducing the actual rate from r_0 to, e.g., $r_0(1 - n_i)$, since a jump to site i can only occur if this site is free. Also, the exit rate from the right ($i = 14$) is assumed to be r_0 . Note that here we have neglected kink-antikink interactions in the system, i.e., the annihilation and spontaneous formation of kink-antikink pairs. These processes can be safely neglected throughout the full range of forces. For small forces, there is seldom a defect present; and at large forces, only the probability of the kink formation is increased because of enhanced injection from the left.

At equilibrium, the left-hand sides of Eqs. 24–26 become zero, and one finds

$$\langle n_{14-i} \rangle = (i + 1)\langle n_{14} \rangle + \frac{k_0}{r_0}(\langle n_{14} \rangle - 1) \quad (27)$$

for $i = 1, \dots, 13$. Finally, using Eqs. 16 and 17, or $k_{\text{esc}}(f)$ and $k_{\text{inj}}(f)$, we obtain from Eq. 24:

$$\langle n_{14} \rangle = \frac{1 + \left(1 + 13\frac{k_0}{r_0}\right)e^{\frac{fa}{2k_B T}} + 13e^{-\frac{fa}{2k_B T}}}{1 + \frac{r_0}{k_0} + \left(14 + 13\frac{k_0}{r_0}\right)\left(1 + \frac{r_0}{k_0}e^{-\frac{fa}{k_B T}}\right)e^{\frac{fa}{2k_B T}}}. \quad (28)$$

Note that in the absence of an external force, $f = 0$, one has $\langle n_{14} \rangle = k_0/(k_0 + r_0)$ and hence $\langle n_1 \rangle = \langle n_2 \rangle = \dots = \langle n_{14} \rangle$. For a nonvanishing applied force, the density of kinks is tilted, with the probability linearly increasing toward the first position $i = 1$.

We are now in the position to calculate the mean total number of kinks inside the nucleosome, $\langle n_{\text{kink}} \rangle$:

$$\begin{aligned} \langle n_{\text{kink}} \rangle &= \sum_{i=1}^{14} \left[i\langle n_{14} \rangle + \frac{k_0}{r_0}(i-1)(\langle n_{14} \rangle - 1) \right] \\ &= 105\langle n_{14} \rangle + 91\frac{k_0}{r_0}(\langle n_{14} \rangle - 1). \end{aligned} \quad (29)$$

Equation 29 is plotted in Fig. 5 and shows excellent agreement with the simulation results (*triangles*). The plateau value of 7.5 is also reproduced (*inset* in Fig. 5) corresponding to the large force asymptotic of Eq. 28, where $\langle n_{14} \rangle \approx 1/14$ and hence $\langle n_1 \rangle \approx 1$. In that case, another kink can only be injected once the first site is free again, which requires that all the kinks to the right have moved out of the way. Since the dynamics of those other kinks is independent of the external force, one finds the large-force plateau in Fig. 5. Note that this system corresponds to the symmetric exclusion process (38).

We study next the nucleosome sliding velocity as a function of the applied force for the case of random DNA. In Fig. 6, we display the simulation results (*triangles*) that share similar features with the corresponding curve for the mean

number of kinks (Fig. 5). On the mean-field level, the net flux j_{kink} of kinks anywhere inside the nucleosome is the same; e.g., between sites i and $i + 1$, one expects

$$\begin{aligned} j_{\text{kink}} &= r_0 \langle n_i \rangle (1 - \langle n_{i+1} \rangle) - r_0 \langle n_{i+1} \rangle (1 - \langle n_i \rangle) \\ &= r_0 \left[\langle n_{14} \rangle + \frac{k_0}{r_0} (\langle n_{14} \rangle - 1) \right]. \end{aligned} \quad (30)$$

Neglecting kink-antikink interactions (that are unimportant at any value of the applied force), it is straightforward to write down the densities of the antikinks and the resulting flux j_{antikink} of those defects. For very small forces, the contributions of both types of defects will be equally important for the nucleosomal mobility, whereas, for larger forces, the kinks become overwhelmingly dominant. The force-induced mean velocity is then—on the mean-field level—predicted to be given by

$$v(f) = a(j_{\text{kink}} - j_{\text{antikink}}). \quad (31)$$

The resulting curve is displayed in Fig. 6, together with the results of the simulation. There is a reasonably good agreement between the data points and the theoretical curve that is especially good for small and large forces, with the curve slightly underestimating the velocity at intermediate forces.

Let us finally consider the case of DNA with a positioning sequence (diamonds in Figs. 5 and 6). The mean number of defects (Fig. 5) turns out to be rather insensitive to the underlying DNA sequence. This can be easily understood by the fact that the production cost of a defect hardly depends on the position of the nucleosome along the DNA. On the other hand, the overall sliding dynamics of the nucleosome is strongly affected by the energy landscape that is felt by the

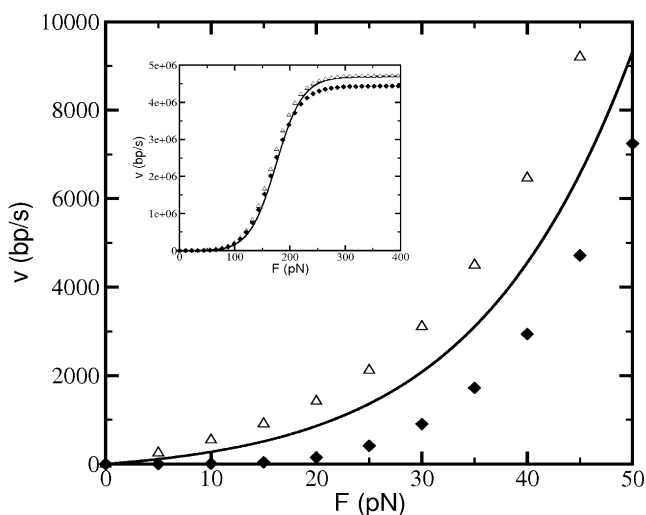


FIGURE 6 Simulation data for the velocity of the nucleosome versus the external force. The open triangles correspond to random DNA and the solid diamonds to a positioning sequence with $A = 9 k_B T$. The solid curve gives the theoretical approach for random DNA from Eq. 31. Our model features a velocity saturation at large forces (inset).

sliding nucleosome—especially for small forces (Fig. 6). This can be understood for small forces by activated barrier crossing (14). For larger forces, again saturation effects come into play, leading to a plateau that is slightly below the random DNA case (inset of Fig. 6).

Collision between RNAP and nucleosome

In this section we consider the coupled system of RNAP and nucleosome. For the isolated entities, the RNAP and the nucleosome, we have already determined the force-velocity relationships in the previous sections. The results are summarized in Fig. 7 for various cases. In a previous publication (16) we have hypothesized that the resulting velocity of the coupled system can be determined from the intersection of the corresponding curves. We would therefore predict from Fig. 7 that the resulting transcription velocity would be $\bar{v}_{\text{RNAP}} \approx 30$ bp/s for $A = 0$ (the same value as for an isolated RNAP) and $\bar{v}_{\text{RNAP}} \approx 26$ bp/s for $A = 9 k_B T$, independent of the underlying mechanism (BR or PS). Now we have a model with a microscopic description that allows us to test this hypothesis.

We start our stochastic simulation at time $t = 0$ with the RNAP at $x = 0$ and place the nucleosome at a free distance of $x = 10$ bp in front of the RNAP. The expression free-distance means here the extra distance beyond the distance L_0 , the distance at physical contact between the RNAP and the nucleosome. Fig. 8 shows distributions of nucleosome positions averaged over 500 ensembles for five different times, $t = 0, 1, 3, 5,$ and 7 s, for the BR and PS mechanism acting on DNA templates with $A = 0$ and $A = 9 k_B T$. The nucleosome distributions for the case $A = 0$ look very similar for the two mechanisms (PS and BR) and after a time of

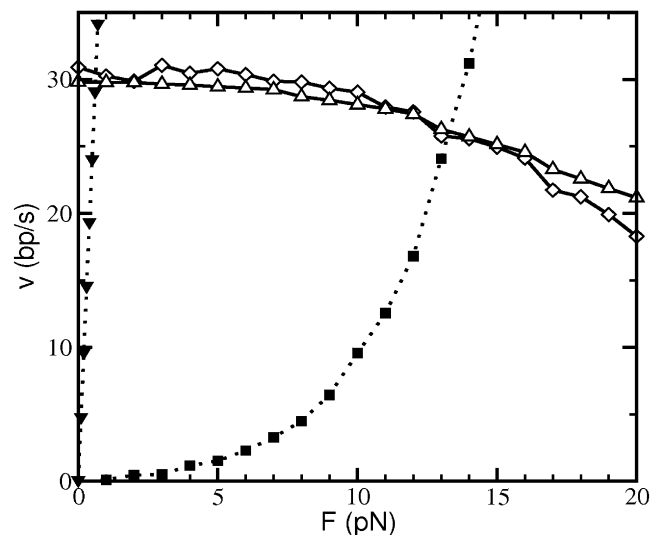


FIGURE 7 Force-velocity relations of isolated RNAPs and of single nucleosomes. The open diamonds and the triangles correspond to the behavior of the RNAP powered by PS and BR mechanisms, respectively. The force-velocity relation of the nucleosome is given by the solid upside-down triangles ($A = 0$) and squares ($A = 9 k_B T$).

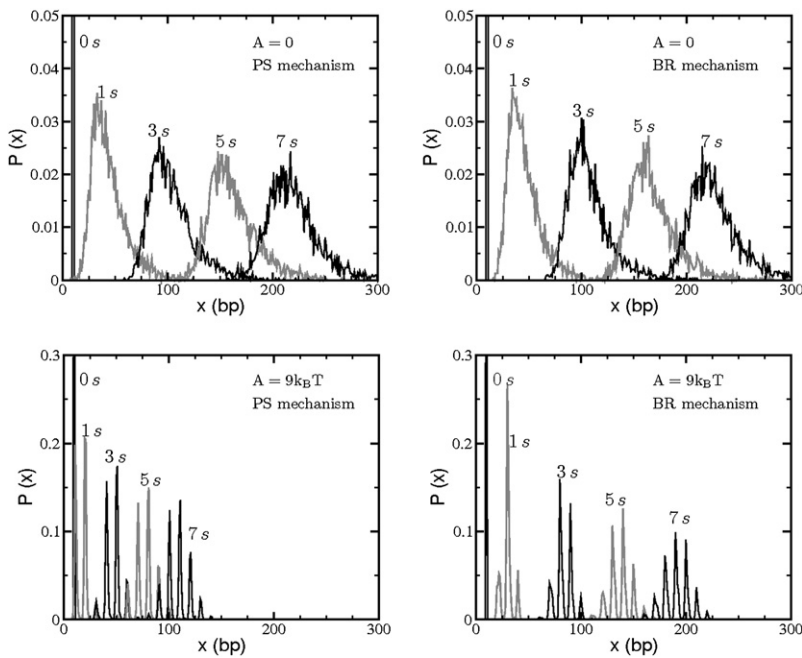


FIGURE 8 Simulation results for the position distributions of nucleosomes that are driven by an RNAP that transcribes to the right. Depicted are distributions for five different times as indicated in the figure. The upper plots show the case of random DNA ($A = 0$) and the lower plots of a positioning sequence with $A = 9 k_B T$. The left plots depict the case of PS RNAP, the right plots of BR RNAP.

$\sim t = 7$ s, a stationary nucleosome distribution that moves forward with a constant velocity is achieved. The distributions are strongly affected by the presence of a positioning sequence that manifests itself through oscillations with a 10-bp periodicity. Visual inspection of the $A = 9 k_B T$ distributions shows already that the speed of the nucleosome in front of the two types of enzymes is substantially different, with the BR RNAP being much more effective in pushing the nucleosome forward. This indicates already that the intersection method does not work well—at least for one of the two mechanisms.

The trajectories of the RNAP together with the nucleosome are shown in Fig. 9 for the PS mechanism ($A = 0$, top and $A = 9 k_B T$, bottom) and in Fig. 10 for the BR mechanism (again, $A = 0$, top and $A = 9 k_B T$, bottom). In all cases, we show the position of the nucleosome and that of the front and catalytic site of the RNAP. We depict the positions such that the nucleosome and the F-site are on top of each other when the RNAP just gets into physical contact with the nucleosome. For the case of random DNA, the nucleosome is diffusing very fast as compared with the slow movement of the RNAP. The fraction of time when the nucleosome is in contact with the RNAP is then very small, and the trajectories of the RNAP (upper plots of Figs. 9 and 10) are thus hardly perturbed by the presence of the nucleosome and look like the trajectories for isolated RNAPs (Fig. 3). This changes dramatically when the nucleosome is positioned (bottom plots of Figs. 9 and 10). As already seen in Fig. 8, the nucleosome is most of the time found in preferred positions 10-bp apart from each other. It usually has no time to escape from such a position before the RNAP reaches it. Once the RNAP is in contact with the positioned nucleosome, the motor protein stalls for some time. This is espe-

cially pronounced for the PS mechanism where the front site F shows often a plateau when in contact with the nucleosome (bottom of Fig. 9). The effect is less pronounced for the BR case (bottom of Fig. 10). Once the RNAP is stuck, the response of the catalytic site is different for the two cases. In the PS case, the site C does not move forward any further but shows wild oscillations around a mean value. In the BR mechanism, however, the catalytic site continues to polymerize—thereby building up a tension inside the RNAP that eventually helps the RNAP to push the nucleosome over the barrier.

The difference in the behavior of the two mechanisms when encountering a positioned nucleosome points toward a different efficiency of the two motor types for the octamer repositioning. The PS mechanism does not have much of a grip onto the DNA and continues spinning (burning ATP) when it encounters the nucleosomal road block. The BR RNAP works pretty much like a macroscopic ratchet: each polymerization step is stored into the mechanical deformation of the RNAP that eventually is large enough to help the nucleosome over the barrier. The overall slopes of the trajectories show clearly that the resulting velocity of the system RNAP-plus-nucleosome is much faster for the BR mechanism (bottom plots of Figs. 9 and 10).

To look further into this, we compare in Fig. 11 the mean velocity of the RNAP behind a nucleosome as a function of the barrier height A in the underlying DNA sequence. As can be seen from the plot, the velocity of the two types of RNAP (BR, triangles connected by solid line; PS, diamonds connected by solid line) is nearly the same on random DNA and slightly below 30 bp/s, the mean-field prediction using the intersection method (Fig. 7). With increasing barrier height A , the velocities decrease, with this effect being

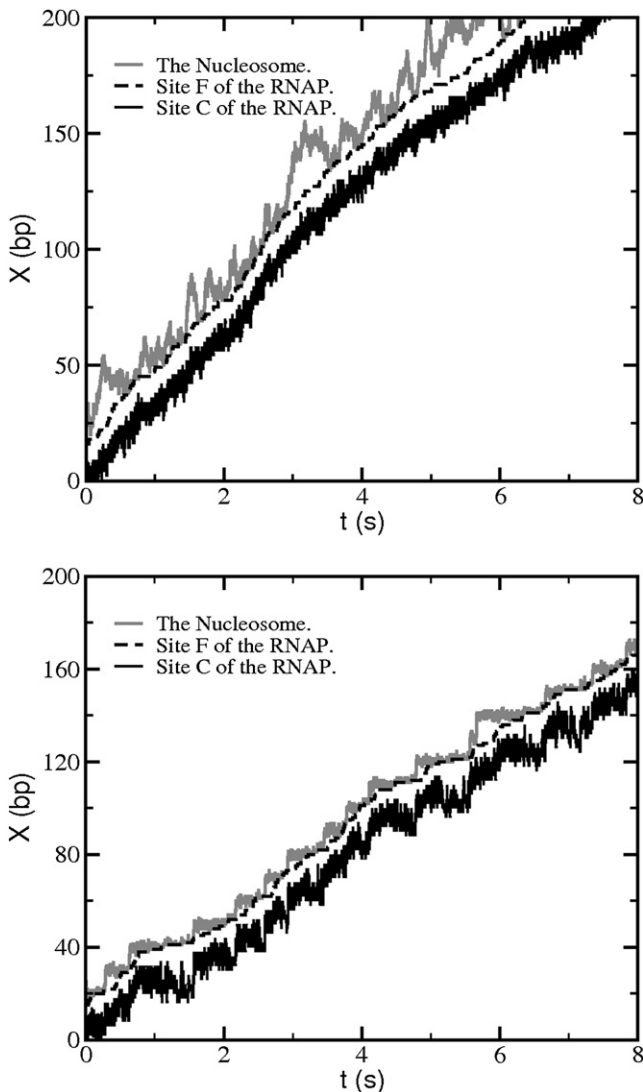


FIGURE 9 Footprint of a PS RNAP behind a nucleosome. The upper plot shows the case of random DNA ($A = 0$) and the lower plot of a positioning sequence with $A = 9 k_B T$.

more pronounced for the PS mechanism. This means that the difference in velocities of the two mechanisms increases, showing, at $A = 9 k_B T$, a velocity difference of 7 bp/s. This has to be compared with Fig. 7, where, for the relevant force-range, no difference between the two mechanisms can be detected. Note that the mean-field prediction of 26 bp/s in the case of RNAP behind a nucleosome with $A = 9 k_B T$ agrees perfectly well with the actual velocity in the BR curve at the same barrier height. Therefore, at first sight it seems that the intersection works very well for the BR mechanism, but breaks down for the PS mechanism at larger barrier heights.

To check this, we determined velocity-versus-force curves for nucleosomes in the presence of various barrier heights (between $A = 0$ and $A = 10 k_B T$; data not shown) and then determined the intersection points with the BR and PS

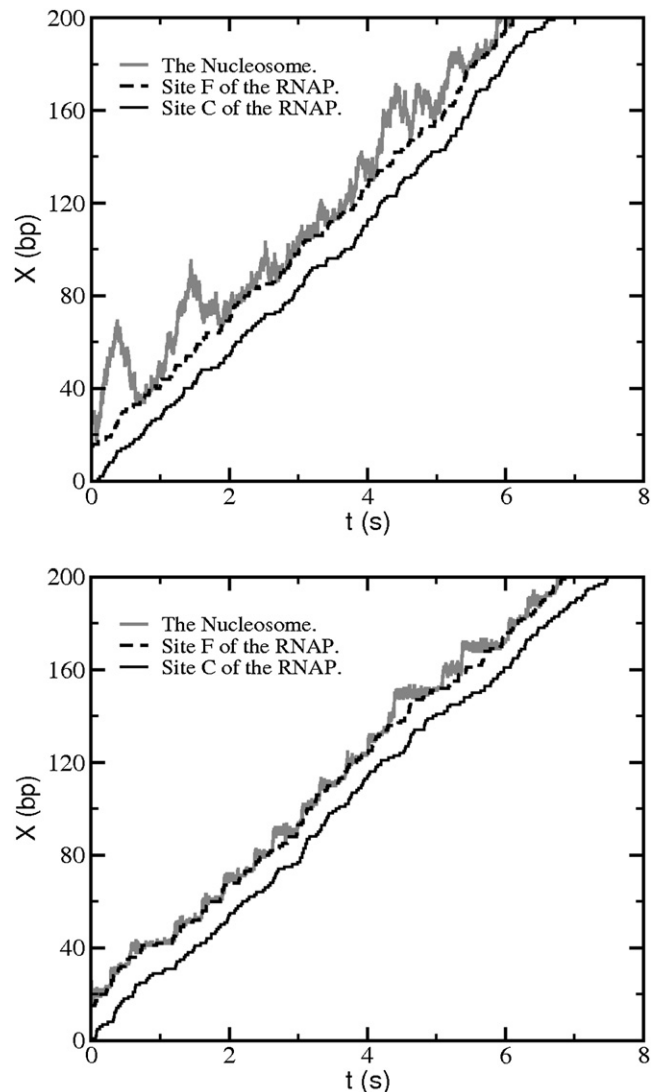


FIGURE 10 Footprint of a BR RNAP behind a nucleosome. The upper plot gives the case of random DNA, $A = 0$, and the lower plot of a positioning sequence with $A = 9 k_B T$.

force-velocity characteristics as done in Fig. 7. The resulting predictions are shown in Fig. 11 as triangles (BR) and diamonds (PS) along dashed lines. Both curves are very close to each other, which is not a surprise since the force-velocity curves of the two mechanisms had been chosen such to be very similar (Fig. 7). Surprising might, however, be how poor the intersection method really works. Looking at the curves, it becomes obvious by eye that only the BR curve happens to intersect with the mean-field curves at $\sim A = 9 k_B T$, the value that we had arbitrarily chosen to represent a positioning sequence. Overall, the method does not work very well—even at small forces where the presence of the nucleosome still slows down the RNAP, especially the one powered by the PS mechanism. Everywhere the BR curve is closer to the mean-field prediction than the PS curve. This might be because the C-site of the PS motor shows large positioning

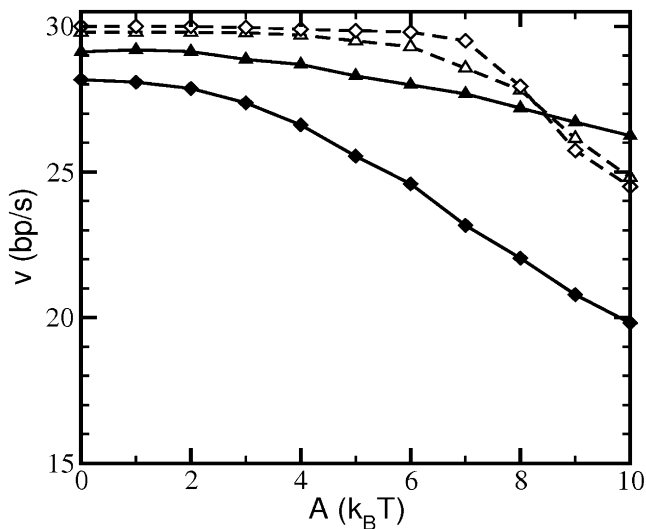


FIGURE 11 Mean velocity of an RNAP behind a nucleosome as a function of barrier height A . The solid triangles correspond to the simulation result of the BR mechanism and the solid diamonds of the PS mechanism. The open triangles and diamonds are the predictions from the intersection method of curves of isolated RNAPs and nucleosomes.

fluctuations, especially when the RNAP is in contact with the nucleosome. Since this is directly tied to large force fluctuations, we expect that the PS mechanism can only poorly be captured by a mean-field approach.

DISCUSSION

In this article, we presented a numeric study of the encounter of a motor protein and a nucleosome. The motor protein might be a transcribing RNAP for which the nucleosome constitutes a roadblock, or it might represent a chromatin remodeling complex that is designed to actively push or pull nucleosomes along DNA. We aimed at giving microscopic descriptions for the motor protein and the nucleosome. Whereas this is relatively straightforward for the nucleosome (nucleosomal mobility most likely results from DNA twist defects), a microscopic description of an RNAP or of a remodeler is difficult at the current stage of research. We chose to make use of the generic toy model for RNAPs of Jülicher and Bruinsma (20) that is set up in such a way that it can operate via the BR or the PS mechanism. In addition, an internal elastic degree of the enzyme is accounted for.

The basic question of our study was: Does the nucleosome repositioning capability of the enzyme depend on the underlying mechanism? To answer this question, we chose the parameters of the RNAP models such that the resulting velocity under a given retarding force is identical (Fig. 4) in the relevant force range $F < 15$ pN. One might then expect that the motor protein pushes a nucleosome with the same speed, independent of the underlying mechanism. Fig. 11 taught us, however, that the performances of the motor protein are very different when encountering a nucleosome.

The BR is much more effective than the PS mechanism: in the latter case, the enzyme does not have a good grip on the DNA, whereas the BR works similar to a macroscopic ratchet.

Another important lesson was: No matter which mechanism underlies transcription, it is not straightforward to predict the behavior of the combined system from the behavior of the isolated objects, RNAP and nucleosome. E.g., predicting the resulting velocity from an intersection of the corresponding curves (Fig. 7) does not work at all, as can be seen in Fig. 11. Because of fluctuations, there is a whole range of forces; to look at only one force value oversimplifies the system.

This teaches us that great care is necessary if we want to come up in the future with more realistic models of, e.g., chromatin remodelers and how they act on nucleosomes. In that context, it might be additionally important to reconsider the modeling of the nucleosome mobility since some experiments indicate that several remodelers base their nucleosome repositioning capability on injection of loops into the nucleosomal DNA (19).

With respect to the RNAP, one might expect that it works based on the BR mechanism since this mechanism is much more effective in repositioning nucleosomes. One has, however, to be aware of the fact that only experiments in which RNAPs encounter single nucleosomes, hint at the RNAP's repositioning capacity. When a polymerase has to push a whole array of nucleosomes, it is likely that it either gets stuck because of a nucleosome traffic jam or that nucleosomes subsequently fall off the template. The latter scenario has indeed been observed in the literature (39,40). However, when a nuclear extract was added it was observed that the nucleosomes seem to stay intact, despite an RNAP that had transcribed through them. It is thus not obvious whether one should expect from RNAPs inherent nucleosome repositioning capacities, since, *in vivo*, other mechanisms seem to facilitate the passage of a transcribing RNAP through nucleosomes.

The mechanism underlying transcription is still under dispute. As mentioned before, some of the recent experimental results (27–29) indicate that an RNAP works by the PS mechanism whereas other experimental data (23,24,26) hint at the BR mechanism. Even if the translocation of the polymerase along the DNA happens with a PS mechanism, the free energy difference between its pre- and posttranslocation states might be such that it can be considered as a weak PS. For instance, Thomen et al. (25) suggests a free energy difference of $\sim 1 k_B T$. Therefore, the behavior of such a motor might also be well captured by the BR model.

To better understand the encounter of an RNAP and a single nucleosome, it will be important to design experiments on long DNA templates and, as a first step, to demonstrate that an RNAP really pushes a single nucleosome forward. Such an experiment might be performed by holding a DNA chain under tension in a micromanipulation

experiment and then by tracking the positions of the fluorescently labeled RNAP and the nucleosome. Comparing this with the force-velocity curves of an isolated RNAP (see, e.g., (37)) and that of an isolated nucleosome (determined, e.g., from a setup where the force is directly applied to the nucleosome) will give us valuable insights into the mechanisms underlying RNA transcription and nucleosome repositioning. We expect the PS mechanism to manifest itself through plateaus in the RNAP trajectory (reflecting contacts with a positioned nucleosome, Fig. 9, bottom) and through a poor performance of the intersection method (Fig. 11). We hope that our theoretical study will be of help in interpreting such experiments.

We are thankful to G. T. Barkema, C. Dekker, M. Depken, J. Widom, and G. J. L. Wuite as well as H. Fazli, M. R. Khajepour, M. Maleki, and B. Famudi for valuable discussions. L.M.-B. acknowledges the hospitality of the Lorentz institute in Leiden, where parts of this work were performed.

REFERENCES

- Luger, K., A. W. Mäder, R. K. Richmond, D. F. Sargent, and T. J. Richmond. 1997. Crystal structure of the nucleosome core particle at 2.8 Å resolution. *Nature*. 389:251–260.
- Schiessel, H. 2003. The physics of chromatin. *J. Phys. Condens. Matter*. 15:R699–R774.
- Polach, K. J., and J. Widom. 1995. Mechanism of protein access to specific DNA sequences in chromatin: a dynamic equilibrium model for gene regulation. *J. Mol. Biol.* 254:130–149.
- Li, G., M. Levitus, C. Bustamante, and J. Widom. 2005. Rapid spontaneous accessibility of nucleosomal DNA. *Nat. Struct. Mol. Biol.* 12:46–53.
- Meersseman, G., S. Pennings, and E. M. Bradbury. 1992. Mobile nucleosomes—a general behavior. *EMBO J.* 11:2951–2959.
- Gottesfeld, J. M., J. M. Belitsky, C. Melander, P. B. Dervan, and K. Luger. 2002. Blocking transcription through a nucleosome with synthetic DNA ligands. *J. Mol. Biol.* 321:249–263.
- Ranjith, P., J. Yan, and J. F. Marko. 2007. Nucleosome hopping and sliding kinetics determined from dynamics of single chromatin fibers in *Xenopus* egg extracts. *Proc. Natl. Acad. Sci. USA*. 104:13649–13654.
- Kulić, I. M., and H. Schiessel. 2004. DNA spools under tension. *Phys. Rev. Lett.* 92:228101.
- Brower-Toland, B. D., C. L. Smith, R. C. Yeh, J. T. Lis, C. L. Peterson, et al. 2002. Mechanical disruption of individual nucleosomes reveals a reversible multistage release of DNA. *Proc. Natl. Acad. Sci. USA*. 99:1960–1965.
- Mihardja, S., A. J. Spakowitz, Y. Zhang, and C. Bustamante. 2006. Effect of force on mononucleosomal dynamics. *Proc. Natl. Acad. Sci. USA*. 103:15871–15876.
- Flaus, A., and T. Owen-Hughes. 2003. Mechanisms for nucleosome mobilization. *Biopolymers*. 68:563–578.
- Schiessel, H., J. Widom, R. F. Bruinsma, and W. M. Gelbart. 2001. Polymer reptation and nucleosome repositioning. *Phys. Rev. Lett.* 86:4414–4417.
- Kulić, I. M., and H. Schiessel. 2003. Nucleosome repositioning via loop formation. *Biophys. J.* 84:3197–3211.
- Kulić, I. M., and H. Schiessel. 2003. Chromatin dynamics: nucleosomes go mobile through twist defects. *Phys. Rev. Lett.* 91:148103.
- Segal, E., Y. Fondufe-Mittendorf, L. Chen, A. Thåström, Y. Field, et al. 2006. A genomic code for nucleosome positioning. *Nature*. 442:772–778.
- Mohammad-Rafiee, F., I. M. Kulić, and H. Schiessel. 2004. Theory of nucleosome corkscrew sliding in the presence of synthetic DNA ligands. *J. Mol. Biol.* 344:47–58.
- Studitsky, V. M., D. J. Clark, and G. Felsenfeld. 1994. A histone octamer can step around a transcribing polymerase without leaving the template. *Cell*. 76:371–382.
- Studitsky, V. M., G. A. Kassavetis, E. P. Geiduschek, and G. Felsenfeld. 1997. Mechanism of transcription through the nucleosome by eukaryotic RNA polymerase. *Science*. 278:1960–1963.
- Cairns, B. R. 2007. Chromatin remodeling: insights and intrigue from single-molecule studies. *Nat. Struct. Mol. Biol.* 14:989–996.
- Jülicher, F., and R. Bruinsma. 1998. Motion of RNA polymerase along DNA: a stochastic model. *Biophys. J.* 74:1169–1185.
- Zhang, G., E. A. Campbell, L. Minakhin, C. Richter, K. Severinov, et al. 1999. Crystal structure of *Thermus aquaticus* core RNA polymerase at 3.3 Å resolution. *Cell*. 98:811–824.
- Wang, H., and G. Oster. 2002. Ratchets, power strokes, and molecular motors. *Appl. Phys. A*. 75:315–323.
- Guajardo, R., and R. Sousa. 1997. A model for the mechanism of polymerase translocation. *J. Mol. Biol.* 265:8–19.
- Bai, L., A. Shundrovsky, and M. D. Wang. 2004. Sequence-dependent kinetic model for transcription elongation by RNA polymerase. *J. Mol. Biol.* 344:335–349.
- Thomen, P., P. J. Lopez, and F. Heslot. 2005. Unraveling the mechanism of RNA-polymerase forward motion by using mechanical force. *Phys. Rev. Lett.* 94:128102–128106.
- Bar-Nahum, G., V. Epshtein, A. E. Ruckenstein, R. Rafikov, A. Mustaev, et al. 2005. A ratchet mechanism of transcription elongation and its control. *Cell*. 120:183–193.
- Landick, R. 2004. Active-site dynamics in RNA polymerases. *Cell*. 116:351–353.
- Temiaikov, D., V. Patlan, M. Anikin, W. T. McAllister, S. Yokoyama, et al. 2004. Structural basis for substrate selection by T7 RNA polymerase. *Cell*. 116:381–391.
- Yin, Y. W., and T. A. Steitz. 2004. The structural mechanism of translocation and helicase activity in T7 RNA polymerase. *Cell*. 116:393–404.
- Mustaev, A., M. Kashlev, E. Zaychikov, M. Grachev, and A. Goldfarb. 1993. Active center rearrangement in RNA polymerase initiation complex. *J. Biol. Chem.* 268:19185–19187.
- Keyser, U. F., B. N. Koeleman, S. van Dorp, D. Krapf, R. M. M. Smeets, et al. 2006. Direct force measurements on DNA in a solid-state nanopore. *Nat. Phys.* 2:473–477.
- Noom, M. C., B. van den Broek, J. van Mameren, and G. J. L. Wuite. 2007. Visualizing single DNA-bound proteins using DNA as a scanning probe. *Nat. Methods*. 4:1031–1036.
- Chou, T. 2007. Peeling and sliding in nucleosome repositioning. *Phys. Rev. Lett.* 99:058105.
- Bustamante, C., S. B. Smith, J. Liphardt, and D. Smith. 2000. Single-molecule studies of DNA mechanics. *Curr. Opin. Struct. Biol.* 10:279–285.
- Gillespie, D. T. 1977. Exact stochastic simulation of coupled chemical reactions. *J. Phys. Chem.* 81:2340–2361.
- Yin, H., M. D. Wang, K. Svoboda, R. Landick, S. M. Block, et al. 1995. Transcription against an applied force. *Science*. 270:1653–1657.
- Wang, M. D., M. J. Schnitzer, H. Yin, R. Landick, J. Gelles, et al. 1998. Force and velocity measured for single molecules of RNA polymerase. *Science*. 282:902–907.
- Evans, M. R., and R. A. Blythe. 2002. Nonequilibrium dynamics in low-dimensional systems. *Physica A*. 313:110–152.
- ten Heggeler-Bordier, B., C. Schild-Poulter, S. Chapel, and W. Wahli. 1995. Fate of linear and supercoiled multinucleosomal templates during transcription. *EMBO J.* 14:2561–2569.
- ten Heggeler-Bordier, B., S. Muller, M. Monestier, and W. Wahli. 2000. An immuno-electron microscopical analysis of transcribing multinucleosomal templates: what happens to the histones? *J. Mol. Biol.* 299:853–858.